3D Automatic Fiducial Marker Localization Approach for Frameless Stereotactic Neuro-surgery Navigation

Lixu Gu[1,2], Terry Peters[2]

[1] Computer Science, Shanghai Jiaotong University, Shanghai, China
gu-lx@cs.sjtu.edu.cn
[2] Robarts Research Institute, London, Ontario, Canada
tpeters@imaging.robarts.ca
www.imaging.robarts.ca/igns

Abstract. Although frameless stereotactic neuro-surgical navigation systems are widely used in many neuro-surgical centers around the world, most of the systems still require the user to define the position of fiducial markers manually from patient scans, a procedure that is tedious, time consuming and often inaccurate. Some researchers have addressed this problem, but they acknowledge that their 2D image processing approach has limitation. We propose a new automatic approach for 3D localization of the fiducial markers, which provides higher 3D localization accuracy, and is independent of the geometry of the marker. Our approach includes three steps. First, sets of 3D morphological operations are employed to extract the candidate fiducial markers as the "seeds". Then a "conditional dilation" technique is employed to reconstruct the regions of fiducials from the "seeds" which are sifted by several knowledge-based rules. Lastly, the intensity-weighted centroid of each extracted fiducial region is calculated as our final fiducial position. The approach is validated by simulated datasets and a CT phantom scan where the average *Fiducial Localization Error* (FLE) is 0.37mm and 0.31mm, respectively.

1 Introduction

When performing minimally invasive surgical interventions, the surgeon's direct view is restricted. Recent progress in computerized imaging techniques has provided pre- and intra-operative images which are exploited to obtain information about the interior of the body. This has increased the use of minimally invasive techniques in general and in brain surgery [1] in particular. Image-guide procedures [2,3] are being employed with increasing frequency in the operating room.

A fundamental requirement for image-guided surgery is that the preoperative images be precisely registered with the patient. Many stereotactic systems employ a frame to satisfy the need for accurate co-registration and probe guidance. However, this approach is often limited since the presence of the frame can be a physical constraint during surgery. The use of computer-based tracking systems using skin mounted or implantable markers provide us with means to address this limitation. These so-called "frameless" stereotactic systems provide the surgeon with naviga-

G.-Z. Yang and T. Jiang (Eds.): MIAR 2004, LNCS 3150, pp. 329-336, 2004.

tional information, relating the location of instruments in the operative field to preoperative image data without the use of a frame.

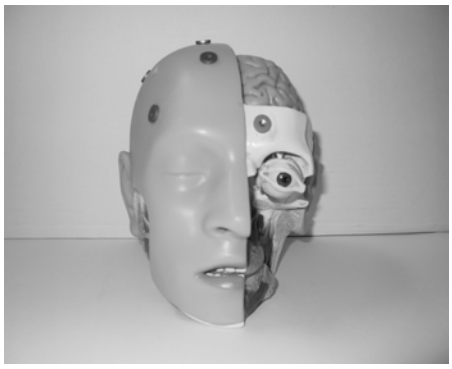

Fig. 1. Fiducial markers attached to a head phantom

There are four different techniques used in co-registration of current frameless stereotactic systems [4]: Point-based methods; Edge methods; Moment methods and "Similarity criterion optimization" methods. Point-based methods using fiducial markers are considered to be quick and reliable [5], and represent the most commonly used approaches.

Several kinds of fiducial markers are employed in current image-guided surgery systems. Some of them are rigidly implanted in the skull [6], but are both time-consuming to apply (requires a separate surgical procedure) and painful for the patient. An alternative to implanted marker is the fiducial that is attached to the skin on the patient's head. An example of this kind of marker (Aesculap -- Tuttlingen, Germany) attached on a phantom head is shown in Fig.1.

We employ the term *Fiducial localization* as the determination of the centroid of a fiducial marker in the acquired image. Wang et al [7] described a method to localize the implanted fiducials using a knowledge-based technique, which is limited to 2D image processing and fiducial markers of a particular geometry. In this paper, we propose an automatic fiducial localization approach using a set of fully 3D morphological techniques. The approach is validated using simulated datasets and a phantom CT scan. Furthermore, our method is not restricted to a particular geometry of fiducial marker.

The rest of the paper is organized as follows: in section 2, after a brief review of mathematical morphology, we describe a fiducial marker detection algorithm using 3D morphological segmentation techniques. In section 3, an intensity-weighted centroid is introduced to determine the fiducial positions, and experiments using both simulated datasets and a CT phantom scan are implemented to validate the proposed approach in section 4.

2 Morphological Treatment for the Detection of Fiducial Markers

2.1 Morphological Operations

Mathematical morphology is a powerful technique for the quantitative analysis of geometrical structures. It consists of a broad and coherent collection of theoretical concepts, nonlinear signal operators, and algorithms aimed at extracting objects from images.

We define a 3D image f as a subset of the 3D Euclidean space ($f \in \mathbf{R}^3$), and a 3D structuring element $k \in \mathbf{R}^3$. The four basic operations can be defined as follows:

$$\text{Dilation:}\quad f \oplus k = \bigcup_{b \in k} (\{a + b \mid a \in f\}) \tag{1}$$

$$\text{Erosion:}\quad f \ominus k = \bigcap_{b \in k} (\{a - b \mid a \in f\}) \tag{2}$$

$$\text{Opening:}\quad f \circ k = (f \oplus k) \ominus k \tag{3}$$

$$\text{Closing:}\quad f \bullet k = (f \ominus k) \oplus k \tag{4}$$

Many other morphological algorithms are derived from these four operations. *Top-hat* transformation (shown in Fig.2) and *Conditional Dilation* (*C-Dilation*) are two typical algorithms employed in our approach for feature extraction and region reconstruction, respectively. They are defined as:

$$\text{Top-hat:}\quad T(f,k) = f - (f \circ_{gray} k) \tag{5}$$

$$\text{C-Dilation:}\quad B_i = (B_{i-1} \oplus k) \bigcap | f |_G \qquad (B_i \in R^3, i = 1,2,\ldots). \tag{6}$$

Here, $\circ_{gray}$ denotes an Opening operation on a grayscale image, and $| f |_G$, the *mask* of the operation, is the result of a threshold operation using gray level *G*. The iteration in (6) is repeated until there is no change between B_{i-1} and B_i.

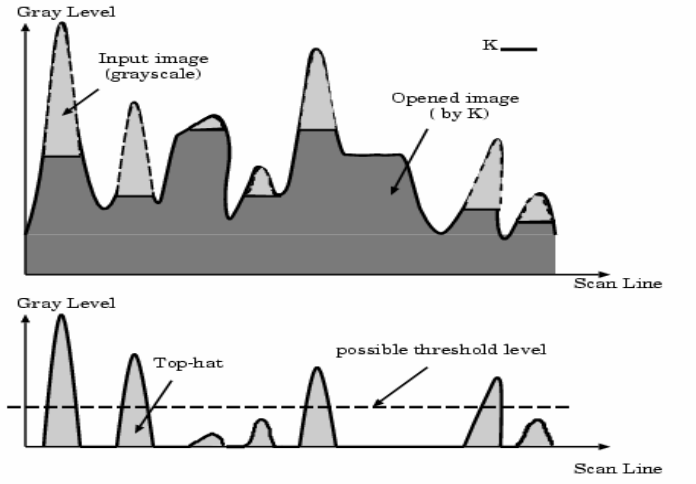

Fig. 2. Top-hat transformation in one dimension. Where dark gray area in upper figure stands for opened image, and the difference between the source and opened images is depicted in the lower figure as the TT result.

3 Fiducial Marker Detection

Our fiducial marker detection algorithm is based on the 3D morphological segmentation techniques outlined above. Processing is divided into three steps: candidate fidu-

cial marker region detection, fiducial marker seed reconfirmation and fiducial marker region recovery.

The first step is designed to detect fiducial marker regions from an entire 3D data set using a top-hat transformation (TT). Since the fiducial markers are designed to present a high intensity level in the input data set and have a standard dimension, the TT can effectively detect them using a 3D spherical structuring element with a size just greater than the largest dimension of the fiducial markers. This detection approach is independent of the shape information of the fiducials. A concept description of the TT function is shown in Fig.2 and defined by equation (5). After we calculate the $T(f,k)$, it is threholded into a binary image $|T|_{G1}$ to distinguish the fiducials from other parts of the image. The intensity level G_1 is determined by the histogram of the TT result $T(f,k)$. Then a binary Opening operation using a spherical structuring element with a diameter of 3 is employed to reduce the remaining noise. This procedure provides us with our candidate fiducial "seeds". The entire processing can be interpreted as a 3D sphere employed to search the 3D input data space to find the objects within a specific high intensity level and with a size smaller than the sphere.

To avoid missing detected fiducial seeds, we confirm every fiducial candidate in the second step, using the following criteria:

1. The distance between every two fiducial seeds should be larger than a constant D. Since fiducial markers are required to be distributed as evenly as possible over an approximately spherical surface, seeds with spacing smaller than D are considered as error candidates which need to be further identified by the next criterion.
2. The intensity of the fiducial seeds in the source image should be in the same range. Since the fiducial markers are made of the same material, a fiducial candidate with an intensity value out of the reasonable range is considered to be an artifact. We note that for MR images, the image should be corrected for rf-inhomogeneities, to ensure that this condition is met.

Such erroneously detected seeds R_{error} are discarded during this step and the final entries E are stored:

$$E = |T(f,k)|_{G1} \circ k_{sphere\_3} - R_{error} \quad , \tag{7}$$

which are pushed into the next step to accurately define the fiducial regions.

During the threshold operation in TT and the noise reduction processing in equation (7), parts of the fiducial contours are destroyed. A morphological "C-Dilation" algorithm is then employed to recover these lost regions. The concept of the *c-dilation* function is defined as equation (6), where the *mask* is defined as $|f|_{G0}$ when the starting *Marker* $M = B_0 = E$ in the iteration. The threshold level G_0 employed here is determined by a histogram analysis of the source image. For CT, G_0 is set to a value just higher than that of bone value resulting a *mask* containing the complete fiducial regions. When the condition of $B_i = B_{i-1}$ is satisfied, the iteration stops automatically, and the final fiducial regions are obtained accurately.

4 Localization Approach

The only assumption we make about the fiducial markers is that they incorporate a spherical depression, matched to a probe tip, which is precisely located at the centroid of the marker. In this manner, accurate identification of the fiducial centroid will at the same time identify the position located by a probe.

Intensity-weighted centroids of each extracted fiducial marker region are used as our fiducial localization results. Intensity weighting implies that the voxel coordinates of the fiducial components are weighted by their intensity. First, the final extracted binary fiducial regions are converted to gray scale by a voxel-based multiplication with the source image. Then the centroid coordinates (X, Y, Z) of the intensity weighted fiducial regions are calculated separately:

$$X = \frac{\sum_{i=0}^{i\max} x_i A(x_i)}{\sum_{i=0}^{i\max} A(x_i)}; \qquad A(x_i) = \sum_{j=0}^{j\max}\sum_{k=0}^{k\max} I(x_i, y_j, z_k) \tag{8}$$

$$Y = \frac{\sum_{j=0}^{j\max} y_j A(y_j)}{\sum_{j=0}^{j\max} A(y_j)}; \qquad A(y_j) = \sum_{i=0}^{i\max}\sum_{k=0}^{k\max} I(x_i, y_j, z_k) \tag{9}$$

$$Z = \frac{\sum_{k=0}^{k\max} z_k A(z_k)}{\sum_{k=0}^{k\max} A(z_k)}; \qquad A(z_k) = \sum_{i=0}^{i\max}\sum_{j=0}^{j\max} I(x_i, y_j, z_k) \tag{10}$$

Here, $I(x_i, y_j, z_k)$ is the intensity value of a voxel in the fiducial region, and *imax*, *jmax* and *kmax* are the numbers of voxels in the X, Y, Z directions in a fiducial region respectively.

5 Validation

5.1 Modeling Study

To validate the proposed approach, we created a series of 3D volume datasets with ten model fiducial markers in each, for use in a simulation experiment. The size of each dataset was $512\times512\times120$ with *1mm* spacing between pixel centers. We employ a cylinder-shaped object with radius r = *6mm* and height h = *4mm* as the fiducial marker, which is the exact dimension of a typical real fiducial marker shown in Fig.1. The whole modeling processing is described as follows.

After the 3D volume is created, ten fiducial centers, randomly selected in 3D space, are recorded as the target fiducial positions. The ten fiducials are automatically

brought into the data volume one by one in a random manner according to the following algorithm:

1. Create a 20 times enlarged cylinder-shaped fiducial marker in a 300×300 ×300 temporary volume region with a size of $r = 120$ and height $h = 80$, where the center of the fiducial is exactly at the center position of the temporary region. This enlargement is designed to model the fiducials more precisely.
2. Rotate the fiducial marker randomly in three directions.
3. Shrink the whole temporary region back to the original dimension with *1mm* pixel distance. We assign the average value of every 20 voxels, to the new corresponding voxel in the shrunken region where the model fiducial marker is finally created. This step simulates the partial volume phenomenon that occurs in practice.
4. Place the created fiducial back to the 3D volume dataset at the position of the corresponding fiducial center.
5. Repeat for all markers in the volume.

In the second step, we blur the created dataset by a *normal distribution* convolution kernel:

$$g(x) = \frac{1}{\sqrt{2\pi}\delta}\exp[-\frac{1}{2}(\frac{x-m}{\delta})^2], \tag{11}$$

where, we set $m = 0$, and δ range from 0.5 to 2.0 to evaluate the effect of different image resolutions. The convolution which is accomplished in 3D space, is defined as follows:

$$f[m,n,o] \otimes g[i,j,k] = \sum_{a=0}^{i-1}\sum_{b=0}^{j-1}\sum_{c=0}^{k-1} f[m-a,n-a,o-c]g[a,b,c] \tag{12}$$

5.2 Phantom Study

A CT scan using the head phantom shown in Fig.1 was employed to further validate our proposed approach, and in particular to demonstrate that our thresholding and morphological operations could robustly separate the markers from underlying structures. This image contains 45 slices with 3mm thick; each slice contains 512×512 pixels of 0.48mm spacing; 8 cylinder-shaped fiducials are randomly attached to the phantom surface, where a concave pivot is located at fiducials' center for pointer rest. Three enlarged cross section views of an example fudicial (#2) are shown in Fig.3, where the highlighted dots labeled with number "2" indicate the automatically detected fiducial position using our proposed approach. Detected fiducial markers with labels can also be identified from the 3D volume viewport.

5.3 Experimental Results

Experiments using a series of model datasets and a CT phantom scan were implemented to evaluate our proposed algorithm. Model datasets include an *in-plane* (without rotation) *fiducial dataset* (**IPFD**), a *dataset without blur* (**DWOB**), four

datasets with blur ranged from $\delta = 0.5$ to 2.0 (**DWB0.5 ~ DWB2.0**), and a *full dataset with rotation and blur* ($\delta = 1.0$) (**FDRB**). *Fiducial Localization Error* (**FLE**) [6] is employed here to measure the accuracy of the proposed fiducial localization approach, which is defined as the Euclidean distance (in mm) between *detected fiducial position* (DFP) and the randomly selected *target fiducial position* (TFP). For the phantom scan, we employ manually defined fiducial position as the TFP when the automatically detected fiducial position as the DFP. The results are shown in Tab.1, where FM1 ~ FM10 refer to the 10 fiducial markers in the experimental datasets.

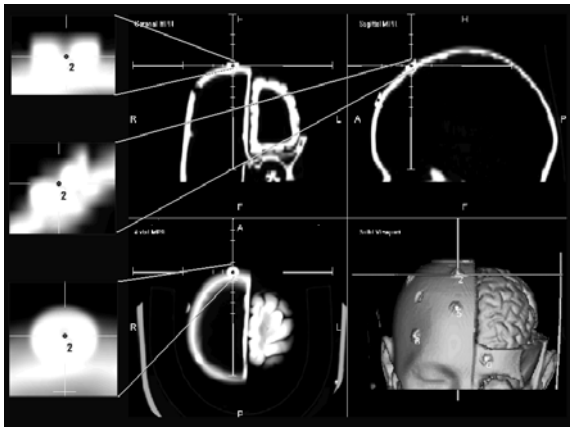

Fig. 3. Fiducials in a CT phantom scan with their TFP

Table 1. Fiducial localization errors (FLE) (in mm)

FLE (MM)	**FM_1**	**FM_2**	**FM-3**	**FM_4**	**FM_5**	**FM_6**	**FM_7**	**FM_8**	**FM_9**	**FM_10**	Average
IPFD	0.29	0.16	0.24	0.33	0.23	0.39	0.29	0.35	0.22	0.26	0.27
DWOB	0.42	0.37	0.49	0.34	0.39	0.19	0.46	0.44	0.36	0.38	0.38
DWB0.5	0.32	0.39	0.45	0.4	0.53	0.19	0.41	0.42	0.47	0.32	0.39
DWB1.0	0.41	0.23	0.53	0.42	0.37	0.48	0.27	0.43	0.35	0.42	0.39
DWB1.5	0.37	0.49	0.33	0.21	0.54	0.38	0.5	0.44	0.32	0.35	0.39
DWD2.0	0.35	0.41	0.39	0.46	0.48	0.35	0.42	0.43	0.23	0.46	0.40
FDRB	0.43	0.29	0.39	0.35	0.34	0.44	0.52	0.35	0.38	0.41	0.39
Average	0.37	0.33	0.40	0.36	0.41	0.35	0.41	0.41	0.33	0.37	0.37
Phantom	0.3	0.2	0.4	0.3	0.4	0.2	0.3	0.4	--	--	0.31

6 Discussion

The 3D localization technique for fiducial markers described in this paper is based on full 3D morphological segmentation algorithms, which reduces the dependence on the shape and the orientation of the 3D fiducial markers. In contrast, the 2D segmentation algorithm described in [7] depends on the orientation of the marker, and the orientation has an effect on the shape of the 2D cross section. Moreover, it may result in a marker cross-section not being identified.

We are undertaking further experiments using both the phantom and patient CT and MRI scan to validate the proposed approach, where a variety of fiducial marker geometries will be tested, and validated against frame-based localization approaches.

7 Conclusion

An automated fiducial marker localization algorithm is proposed for image registration in frameless stereotactic neuro-surgery navigation. The approach is designed to work with different types of fiducials using multi-modality images. The algorithm is validated by a series of simulated datasets and a CT phantom scan showing FLE is in the order of 0.37mm and 0.31mm, respectively.

References

1. A. D.Salles, R.Lufkin (eds), "*Minimally Invasive Therapy of the Brain*", Thieme, New York, Stuttgart, 1997.
2. F.A.Jolesz, "*Image-guided Procedures and the Operating Room of the Future*", Radiology 204:601-612,1997.
3. K.W.Finnis, Y.P.Starreveld, A.G.Parrent, T.M.Peters, "A 3-Dimensional Database of Deep Brain Functional Anatomy, and Its Application to Image-Guided Neurosurgery", In MICCAI 2000, 1-8, Oct. 2000.
4. C.R.Maurer, J.M.Fitzpatrick, "*A Review of Medical Image Registration*", Interactively active Image-Guided Neurosurgery, a book edited by R.J.Maciunas, Park Ridge, IL: American Association of Neurological Surgeons, 17-44, 1993.
5. J.West, J.M.Fitzpatrick, M.Y.Wang, B.M.Dawant, C.R.Maurer et al, "*Comparison and evaluation of retrospective intermodality brain image registration techniques*", Journal of Computer Assisted Tomography, 21 (4): 554-566, 1997.
6. C.R.Maurer, J.M.Fitzpatrick, M.Y.Wang, R.L.Galloway, R.J.Maciunas, G.S. Allen, "*Registration of head volume images using implantable fiducial markers*", IEEE Transactions on Medical Imaging, 16:447-462, 1997.
7. M.Y.Wang, C.R.Maurer, J.M.Fitzpatrick, R.J.Maciunas, "*An automatic Technique for Finding and Localizing Externally Attached Markers in CT and MR Volume Images of the Head*", IEEE Transactions on Biomedical Engineering, vol. 43, No.6: 627-637, June 1996.